THE JOURNAL OF PHYSICAL CHEMISTRY Letters

pubs.acs.org/JPCL

Letter

Thermodynamics of Water–Cationic Species–Framework Guest–Host Interactions within Transition Metal Ion-Exchanged Mordenite Relevant to Selective Anaerobic Oxidation of Methane to Methanol

Xianghui Zhang, Cody B. Cockreham, Zhiyang Huang, Hui Sun,* Chen Yang, Oscar G. Marin-Flores, Baodong Wang, Xiaofeng Guo, Su Ha, Hongwu Xu, and Di Wu*

Cite This: *J. Phys. Chem. Lett.* 2020, 11, 4774–4784

Read Online

ACCESS | Metrics & More | Article Recommendations | Supporting Information

ABSTRACT: Low-temperature anaerobic methane conversion to methanol (MTM) using copper ion-exchanged mordenite (Cu-MOR) as the catalyst and water as the sole source of oxygen is promising for sustainable utilization of methane. Integrating *in situ* calorimetric, spectroscopic, and structural methodologies, we report a systematic study on energetics of water–cationic species–framework guest–host interactions as a function of water loading for several mordenites relevant to low-temperature MTM. Notably, the near-zero coverage hydration enthalpy on Cu-MOR is −133.1 ± 6.0 kJ/mol water, which is related to Cu-MOR regeneration using water as oxidant. The copper oxo sites are thermally stable up to 915 °C and remain chemically intact as an oxygen source after complete hydration and dehydration. This study underscores the importance of manipulating the oxidation state and coordination chemistry of transition metal guest species in zeolites by fine-tuning the partial pressure of water as a strategy for rational design, synthesis, and modification of catalysts.

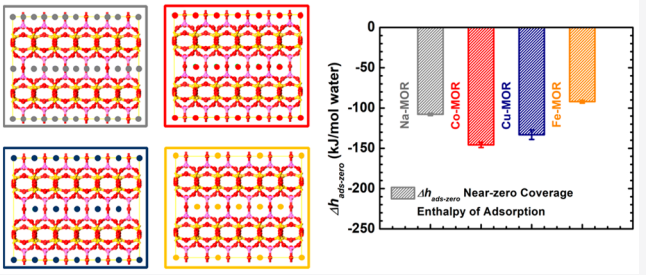

Direct conversion of methane from natural gas and shale gas into liquid organic compounds is desired to produce value-added chemicals and fuels with more effective transportation and storage.[1−7] Current research emphasizes direct partial oxidation of methane using oxygen to oxygenates, such as methanol and formaldehyde, at significantly elevated temperature (~700 °C). Such harsh reaction environments easily lead to complete oxidation of methane to CO_2. Biologically, a family of enzymes, methane monooxygenase proteins (MMOs), selectively oxidize methane to methanol (MTM) using molecular oxygen as the oxidant at ambient temperature.[8−12] The catalytically active centers identified are iron (Fe) for soluble MMO (sMMO)[8,9] and copper (Cu) for particulate MMO (pMMO).[12] These sites have been engineered and replicated in transition metal (M)-exchanged zeolites to catalyze MTM reactions under similar near-ambient conditions, in which sMMO and pMMO are mimicked by Fe- and Cu-exchanged zeolites, respectively.[13−19] The local environment of transition metal sites on the inorganic microporous supports is as complicated as that within enzymatic macromolecules, especially considering the zeolite topology, Si/Al ratio, type of transition metal, and degree of hydration. Moreover, identification of the chemical nature of the transition metal sites and how they interact with water, the reactants, intermediates, and products are essential and critical.

Fundamentally, zeolites are microporous aluminosilicates with corner-sharing tetrahedra (TO_4; T atom = Si, Al) as their building units.[20] T atom substitution of Si^{4+} by Al^{3+} leads to negatively charged frameworks neutralized by cationic guest species ($Si^{4+} = Al^{3+} + 1/n\ M^{n+}$). Charge-balancing cations are usually alkali, alkaline earth and transition metal cations, and quaternary ammonium ions, which are dispersed within the zeolite lattice at specific locations. Typically, as-made aluminosilicate zeolites have Na^+ as the charge-balancing cations that can be further exchanged by other ions, such as Mn^{2+}, Fe^{3+}, Co^{2+}, Ni^{2+}, Cu^{2+}, and Zn^{2+}. The products, transition metal-exchanged zeolites, may serve as catalysts in partial oxidation of methane to methanol,[21−24] biomass conversion,[25−29] and selective catalytic reduction of NO_x.[30−33] On the other hand, the guest cations, surface and internal void space of zeolite framework are all hydrated. The roles water plays in heterogeneous catalysis are multifaceted and complex.[34−46] For example, the redox-relevant properties of metal species confined within zeolites, such as valency and coordination number, can be substantially modified by tuning the degree of hydration.[36−38,44−46] In addition, in MTM

Received: April 30, 2020
Accepted: May 26, 2020
Published: May 26, 2020

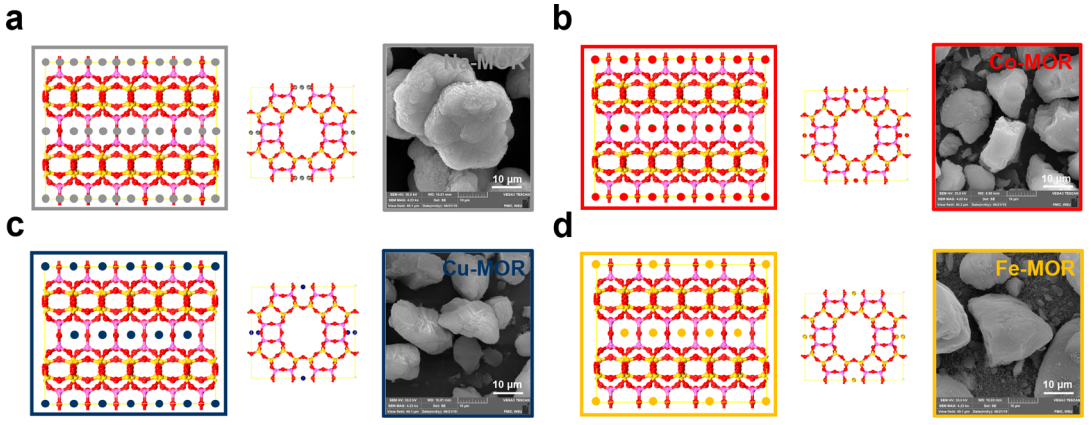

Figure 1. Illustrated structures and morphologies of all M-MOR samples revealed by scanning electron microscopy (SEM): (a) Na-MOR, (b) Co-MOR, (c) Cu-MOR, and (d) Fe-MOR.

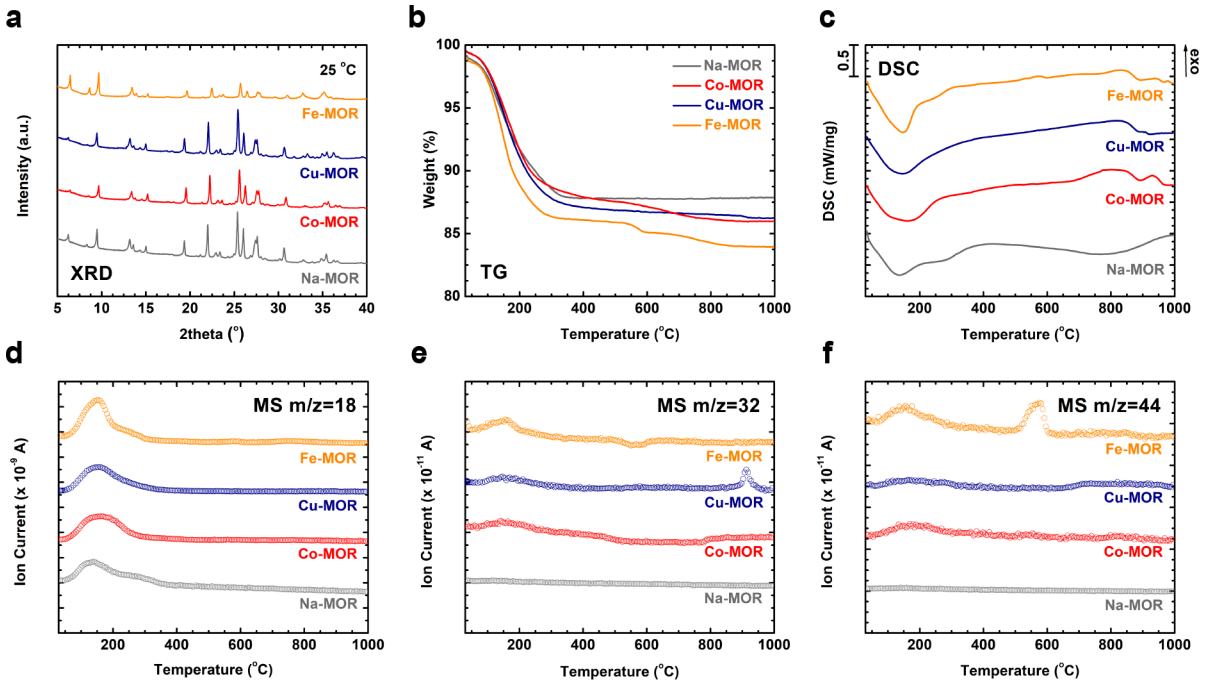

Figure 2. (a) *Ex situ* XRD patterns at 25 °C. (b) TG, (c) DSC, and MS curves: m/z = (d) 18, (e) 32, and (f) 44 of each M-MOR sample. Data were collected from 30 to 1000 °C at 10 °C/min under nitrogen flow (50 mL/min).

reactions, water is known to extract methanol and to reactivate/deactivate the Cu and Fe-exchanged zeolites.[13,15,16,21−23] Recently, using Cu-exchanged mordenite (Cu-MOR) as the catalyst, van Bokhoven and co-workers reported a direct stepwise method that partially oxidizes methane to methanol at low temperature with water serving as the only source of oxygen.[47] In this reaction, water plays unique and critical roles. Specifically, water acts (i) as a reactant to partially oxidize methane, (ii) as a molecular ligand to stabilize the reaction intermediates, and (iii) as an oxidant to regenerate the copper oxo sites within Cu-MOR.[47] Therefore, understanding the hydration behavior as temperature and the degree of hydration vary is critical toward further optimization of "low-temperature" MTM conversion using Cu-MOR as the catalyst and water as the oxygen source. Although the catalytic performance and reaction mechanisms of MTM have been extensively studied spectroscopically and computationally,[4,48,49] the fundamental water−zeolite guest−host interactions are underexplored from an experimental thermodynamic perspective. For example, knowing the near-zero coverage enthalpy of hydration for Cu-MOR could lead to new understanding on the energetic effects during regeneration of $[Cu^{2+}-O^{2-}-Cu^{2+}]^{2+}$ active sites from the inactive $[Cu^{+}\square Cu^{+}]^{2+}$ using water.[47]

Thus far, the thermodynamic studies of ion-exchanged zeolites have been primarily focused on alkali and alkaline earth ion-exchanged zeolites using high-temperature oxide melt solution calorimetry with emphasis on the macroscopic energetics of zeolite formation relevant to geochemistry and material synthesis.[50] Systems studied include zeolite A,[51,52] β,[53] X/Y,[54] and natrolite.[55] The general conclusion is that the hydration energetics, cation−zeolite interactions, and thermodynamic stability of zeolites with the same framework topology and Si/Al ratio are correlated to the average ionic potential of guest cations, Z/r, calculated using $Z/r = \sum x_i(Z/r)/\sum x_i$), in which x_i, Z, and r represent mole fraction, number of cation

https://dx.doi.org/10.1021/acs.jpclett.0c01331
J. Phys. Chem. Lett. 2020, 11, 4774−4784

charge, and ionic radius, respectively. Specifically, as the average ionic potential increases, the average hydration enthalpy derived from thermogravimetry−differential scanning calorimetry (TG-DSC) thermal analysis becomes more exothermic, while the zeolite tends to be less stable reflected by less exothermic enthalpy of formation. Nevertheless, microscopic structural and spectroscopic insights into the simultaneous evolutions on the same family of samples during hydration and/or dehydration using integrated *in situ* methodologies are rarely documented.

Here, to elucidate the roles water plays in Cu-MOR relevant to anaerobic oxidative MTM reactions, and to reveal the thermodynamic basis that distinguishes Cu-MOR from other common transition metal ion-exchanged mordenites (M-MORs) for being an effective and highly stable catalyst to transfer the oxygen atom from water to methane, we performed this study on the water−cationic species−framework guest−host chemistry within a family of M-MOR, including Na-, Co-, Cu-, and Fe-MOR. Integrating thermogravimetry−differential scanning calorimetry−mass spectrometry (TG-DSC-MS) with three powerful *in situ* experimental methodologies, including water adsorption calorimetry, *in situ* diffuse reflectance infrared Fourier transform spectroscopy (*in situ* DRIFTS) and *in situ* X-ray diffraction (*in situ* XRD), we enabled (i) determination of the integral (average) and differential enthalpies of hydration from near-zero water coverage to saturation as a function of water loading; (ii) elucidation of the local chemistry between water molecules and the transition metal species under confinement within the micropores of MOR; and (iii) identification of the macroscopic, structural, and compositional evolutions under thermal treatment in controlled atmosphere. From a thermodynamic perspective, the fundamental knowledge gained here highlights the complex hydration chemistry of Cu-MOR enabling a unique MTM conversion catalyst with high performance under anaerobic reaction environments. The present study will also shed light on transition metal zeolite catalysis in anaerobic MTM conversion, from catalyst pretreatment to regeneration to stabilization of the electronic structures of mildly oxidative transition metal species.

The illustrated structures and representative SEM images for all four M-MOR samples are shown in Figure 1. SEM images reveal typical morphology of MOR. Each Na-MOR particle, which is essentially an aggregate of many cuboid-shaped crystals, appears to be flower-like. Minor morphological degradation is observed for post ion-exchange samples, which does not lead to significant impact on the adsorption and formation energetics.[56] The room-temperature *ex situ* XRD patterns of all samples are presented in Figure 2a. The diffraction data suggest that all samples share an orthorhombic structure, but the peaks of Fe-MOR show a decrease in intensity which is consistent with the observation from its SEM image.

The TG-DSC-MS curves are presented in Figure 2b−f. When TG-DSC-MS is coupled with ICP-MS analysis, the stoichiometries of all M-MOR samples are determined (see Table 1). The TG-DSC-MS profiles suggest a three-stage thermal evolution as a function of temperature. Specifically, in *Stage I*, between 100 and 400 °C, all samples experience major weight loss ranging from 8 wt % (Na-MOR) to 12 wt % (Fe-MOR) associated with broad endothermic DSC peaks (see Figure 2c). According to the MS results in Figure 2d−f, dehydration is responsible for the weight loss in this range.

Table 1. Composition, Molecular Weight (MW), and Cation Concentration (CC) of M-MOR Samples (M = Na, Co, Cu, and Fe) Based on ICP-MS and TG-DSC-MS Results

Sample	Formula	MW (g/mol zeolite)	CC (mmol/g zeolite)
Na-MOR	$0.95Na_2O{\cdot}11.84SiO_2{\cdot}Al_2O_3{\cdot}5.33H_2O$	968.2	1.96
Co-MOR	$0.22Na_2O{\cdot}0.80CoO{\cdot}11.77SiO_2{\cdot}Al_2O_3{\cdot}6.18H_2O$	994.0	0.81
Cu-MOR	$0.18Na_2O{\cdot}0.64CuO{\cdot}11.78SiO_2{\cdot}Al_2O_3{\cdot}5.86H_2O$	977.4	0.66
Fe-MOR	$0.05Na_2O{\cdot}1.87Fe_2O_3{\cdot}15.03SiO_2{\cdot}Al_2O_3{\cdot}9.57H_2O$	1479.1	2.53

DSC, MS, and derivative thermogravimetry (DTG, Figure S1) results all point out that Na- and Fe-MOR feature two dehydration events, suggested by the shoulders in both DSC and MS profiles between 200 and 350 °C, while Co- and Cu-MOR samples exhibit single-step water desorption with broad DSC peaks centered at about 159 and 149 °C, respectively. Notably, for Na-MOR, dehydration in *Stage I* is the only detectable weight loss event between 30 and 1000 °C. According to the TG and MS data presented in Figure 2b,d, the degrees of hydration are 6.11, 7.00, 6.72, and 7.50 mmol/g zeolite for Na-, Co-, Cu-, and Fe-MOR, respectively. Derived from the DSC data, the average dehydration enthalpies (Δh_{des}) are 61.2 ± 1.2, 59.8 ± 0.7, 59.8 ± 0.2, and 58.5 ± 0.5 kJ/mol water for Na-, Co-, Cu-, and Fe-MOR, respectively. Overall, thermal dehydration dominates *Stage I* weight loss. The trace amount of loosely attached or physisorbed O_2 and CO_2 are also liberated in *Stage I* (see Figure 2e,f).

In *Stage II*, between 400 and ∼950 °C, Co-, Cu-, and Fe-MOR show weight loss. In contrast, there is no detectable weight loss for Na-MOR. Fe-MOR exhibits weight loss starting at ∼500 °C (0.9 wt %) accompanied by a weak endothermic event and liberation of CO_2 (see Figure 2b,c,f). This phenomenon appears to be at a similar temperature of amorphous carbonate decomposition and suggests the potential existence of framework-confined iron carbonate species lacking long-range order.[57−59] The gradual weight loss spanning from 400 to ∼800 °C observed for Co-MOR is due to residual water (see Figure 2b,d). Between 700 and 920 °C, relatively weak and broad exothermic peaks were observed for Co-, Cu-, and Fe-MOR (see Figure 2c). Interestingly, the Cu-MOR sample loses 0.2 wt % by releasing O_2 accompanied with a sharp MS peak centered at about 915 °C (see Figure 2e), while above 900 °C, heating Na-, Co-, and Fe-MOR does not result in any measurable weight loss. Therefore, the TG-DSC-MS data in *Stage II* affirm the evolution of CO_2 at about 500 °C, but to confirm the presence of iron carbonate species in Fe-MOR, we conducted spectroscopic analysis using *in situ* DRIFTS (reported below). Moreover, it is also indicated that there are copper oxo clusters in Cu-MOR by the simultaneously release of O_2 at about 915 °C upon thermal decomposition. In *Stage III*, at 1000 °C, other than Na-MOR, all samples become amorphous (see Figure S2).

Water adsorption calorimetry at 25 °C is employed to elucidate the hydration mechanisms of M-MOR samples from a thermodynamic perspective as a function of vapor pressure (see Figure 3). Before water adsorption calorimetry, *in vacuo* dehydration at 350 °C does not result in any detectable phase degradation (see Figure S3). From water adsorption analysis, all samples show *Type II* isotherms with abrupt initial water

https://dx.doi.org/10.1021/acs.jpclett.0c01331
J. Phys. Chem. Lett. 2020, 11, 4774−4784

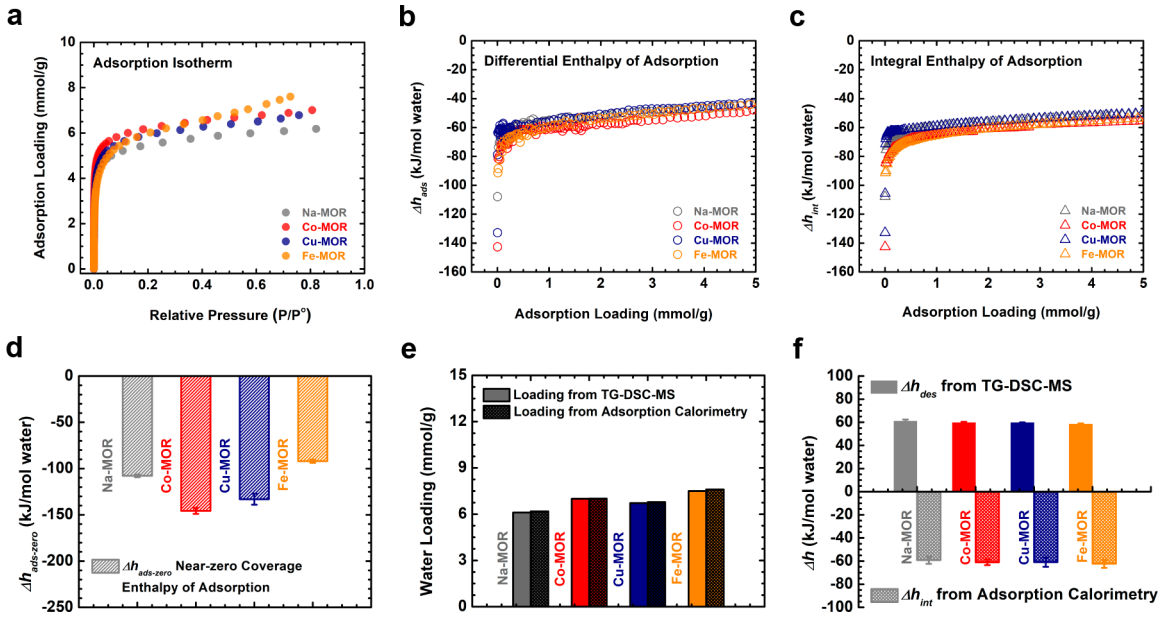

Figure 3. (a) Water adsorption isotherms, (b) differential, (c) integral, and (d) near-zero coverage enthalpies of water adsorption of all M-MOR samples at 25 °C. (e) Water loading and (f) average enthalpies of dehydration and integral hydration enthalpies at 25 °C obtained from TG-DSC-MS thermal analysis and water adsorption calorimetry, respectively.

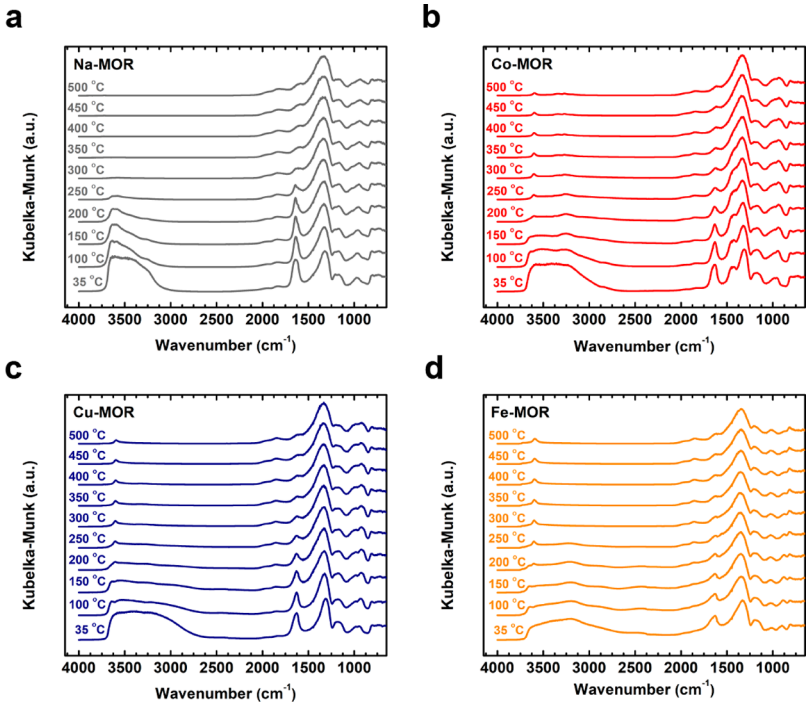

Figure 4. *In situ* diffuse reflectance infrared Fourier transform spectroscopy (*in situ* DRIFTS) spectra of each sample as a function of temperature from 35 to 500 °C under helium flow of 50 mL/min: (a) Na-MOR, (b) Co-MOR, (c) Cu-MOR, and (d) Fe-MOR (see the Supporting Information for a detailed description of the results of Na- and Co-MOR).

uptake, which suggests favorable initial adsorbate−adsorbent binding followed by adsorbate−adsorbate intermolecular interactions (Figure 3a). The steep slopes observed at low partial pressure (P/P^o < 0.015) for all isotherms highlight the strong initial binding between water and M-MOR at near-zero coverage. The differential enthalpies of the water adsorption (Δh_{ads}) are plotted in Figure 3b. The most exothermic, near-zero coverage water adsorption enthalpies ($\Delta h_{ads\text{-}zero}$) are −107.8 ± 1.5, −145.7 ± 3.2, −133.1 ± 6.0, and −92.0 ± 1.8 kJ/mol water, for Na-, Co-, Cu-, and Fe-MOR, respectively (also see Figure 3d). All differential enthalpies of water adsorption curves conclude with a plateau at about −44 kJ/mol water, corresponding to the condensation of bulk water on the hydrophilic external surface of M-MOR. *Ex situ* XRD data in Figure S4 confirm that after water adsorption calorimetry experiments, no detectable structural degradation occurs. Additionally, the overall water uptake for each sample is in excellent agreement with the water content from dehydration

https://dx.doi.org/10.1021/acs.jpclett.0c01331
J. Phys. Chem. Lett. 2020, 11, 4774−4784

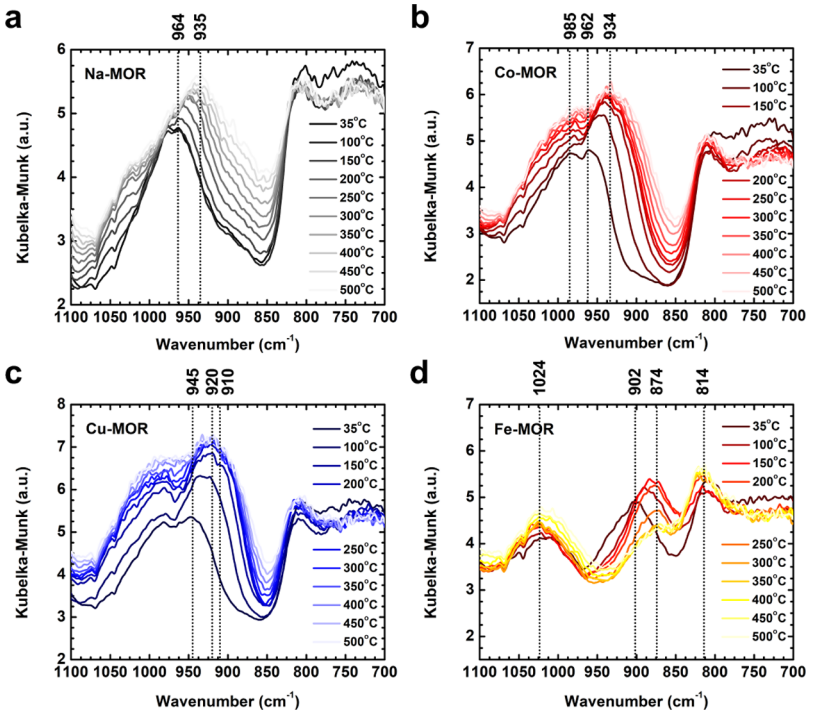

Figure 5. Low-wavenumber (1100−700 cm^{-1}) *in situ* DRIFTS spectra of each sample as a function of temperature from 35 to 500 °C under helium flow of 50 mL/min: (a) Na-MOR, (b) Co-MOR, (c) Cu-MOR, and (d) Fe-MOR (see the Supporting Information for a detailed description of the results of Na- and Co-MOR).

obtained from TG-DSC-MS (see Figure 3e), and the integral enthalpies of adsorption (Δh_{int} in Figure 3c) are consistent with the corresponding enthalpies of dehydration (Δh_{des}, see Figure 3f). To a first-order approximation, the near-zero coverage enthalpy of hydration on Cu-MOR (−133.1 ± 6.0 kJ/mol water) is within the same range as the predicted value by density functional theory (DFT) simulation for the regeneration of hydrated $[Cu^{2+}-O^{2-}-Cu^{2+}]^{2+}$ active sites from the inactive $[Cu^{+}\square Cu^{+}]^{2+}$ using water as the oxidant.[47]

Transition metal ion exchange significantly modifies the degree of hydration, distribution, population of guest cations, and internal space of zeolite frameworks. For M-MOR, once one divalent cation is introduced, two monovalent Na^{+} are exchanged, and the exchange of one trivalent Fe^{3+} substitutes three Na^{+} (Figure 1). The reduction of cation population leads to more internal space to host water. This is reflected by the degree of hydration obtained from TG-DSC-MS (Figure 2b,d) and the total water uptake from adsorption analysis (Figure 3a and e), which are in good agreement. For ion-exchanged zeolites, multiple earlier studies suggest that the enthalpy of hydration at low loading, which generally reflects the interactions between water and cations, is a function of the average ionic potential (Z/r) of the guest cation (see Table S1 for Z/r).[53,54,60,61] As the average ionic potential of the guest cation increases, the near-zero enthalpy of adsorption becomes more exothermic, suggesting stronger water−cation binding. As such, it is logical to expect that the near-zero enthalpy of hydration ($\Delta h_{ads\text{-}zero}$) would become more exothermic following the order of Na-, Cu-, Co-, and Fe-MOR (see Figure 3b,d and Table S1). However, surprisingly, our calorimetry data suggest that $\Delta h_{ads\text{-}zero}$ tends to be more exothermic following the sequence of Fe-, Na-, Cu-, and Co-MOR. Considering the intrinsic complexity of transition metal cations, especially the presence of copper oxo clusters in Cu-MOR and iron carbonate species in Fe-MOR, here, it is necessary to revise the analysis on the relations between $\Delta h_{ads\text{-}zero}$ and Z/r.

To determine the bonding specifics of M-MOR hydration and the chemical nature of cationic guest species, we carried out *in situ* DRIFTS study as a function of temperature from 35 to 500 °C under helium flow of 50 mL/min. The full-range *in situ* DRIFTS spectra of all samples are presented in Figure 4. There are two key parameters which determine the band frequency and intensity. Specifically, they are (i) the mass of the confined guest species and (ii) the force constant of the $O-M^{n+}$ bond, which is governed by the ion valency and by the type and number of ligand in the coordination sphere. As temperature increases, the infrared (IR) peaks at 3620 and 1640 cm^{-1} assigned to the stretching vibration and bending modes of O−H, respectively, tend to be narrower and disappear at 300 °C. The signal at 1350 cm^{-1} is from the $\nu 1$ asymmetric stretching mode of Si−O−Si of the MOR framework. On the other hand, the IR peaks reflecting the nature and impacts of transition metal guest species reside in low wavenumbers from 1000 to 900 cm^{-1}, within which the presence of a small fraction of heteroatoms will induce detectable subtle IR absorption.[62−68] The peaks in this wavenumber range are assigned to the asymmetric stretching mode of a modified Si−O−Si structure caused by the interaction between flexible zeolitic lattice and bare cations, rather than to that of the M−O bond. Evidence to support the assignment is that the peaks shift to higher wavenumbers or disappear when extraframework ligands such as NH_3, CO, and H_2O interact with the bare cations because the interaction compromises the deformation of the Si−O−Si bond.[62,63]

Low-wavenumber (1100 to 700 cm^{-1}) *in situ* DRIFTS spectra of Na- and Co-MOR samples are plotted in Figure 5a,b, which are described in the Supporting Information. For

https://dx.doi.org/10.1021/acs.jpclett.0c01331
J. Phys. Chem. Lett. 2020, 11, 4774−4784

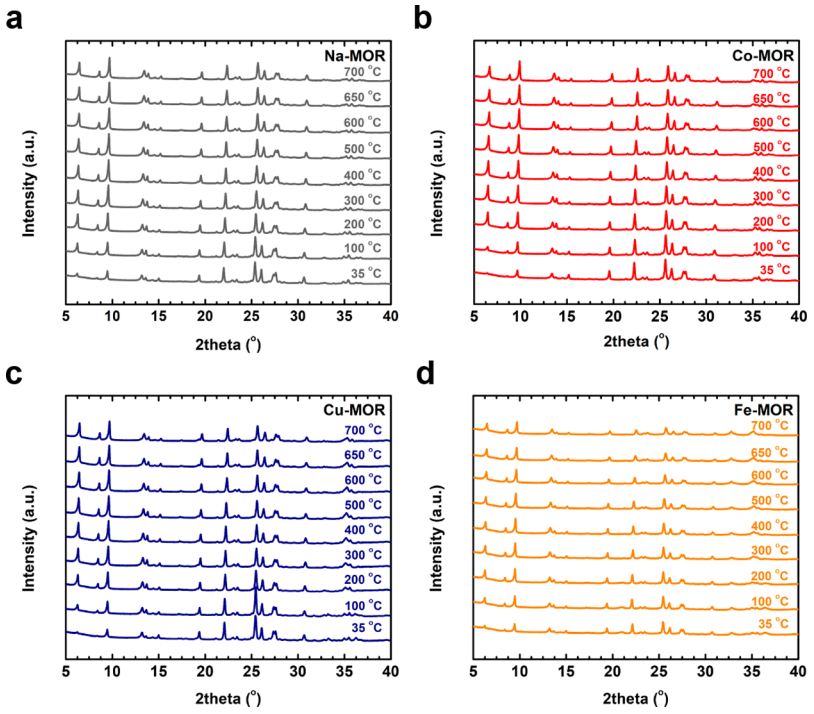

Figure 6. *In situ* X-ray diffraction (*in situ* XRD) patterns of all M-MOR samples as a function of temperature from 35 to 700 °C under helium flow (50 mL/min): (a) Na-MOR, (b) Co-MOR, (c) Cu-MOR, and (d) Fe-MOR. Data were collected from 5 to 40° (see the Supporting Information for a detailed description of the results).

Cu-MOR, at room temperature there are two major signals at 980 and 945 cm^{-1} at low wavenumber (see Figure 5c). As temperature increases to 200 °C, the signal at 945 cm^{-1} shifts to 920 cm^{-1} and presents increased intensity due to dehydration. According to various reports, the peak at 920 cm^{-1} is ascribed to ν_{asym}(Si−O−Al) (asymmetric vibration) perturbed by Cu^{2+} ions, while the signal at 945 cm^{-1} reflects the hydroxylated Cu^{2+} ion, $[Cu^{2+}OH^{-}]^{+}$.[63−65,67,68] Further thermal dehydration of $[Cu^{2+}OH^{-}]^{+}$ at ∼200 °C leads to simultaneous formation of $[Cu^{2+}{-}O^{2-}{-}Cu^{2+}]^{2+}$ with very weak signal at 910 cm^{-1} (not shown in our figure) due to its high stability indicated by our TG-DSC-MS data and rigidity reported in the literature.[47,65,69−72] Although not observed in our *in situ* DRIFTS experiments, it has been reported that thermal reduction of Cu-MOR under vacuum at temperatures above 200 °C leads to progressive reduction of Cu^{2+} to Cu^{+} at 980 cm^{-1}.[47,65,69−72] Such *in vacuo* autoreduction is better monitored by IR spectroscopy using CO or NO as the molecular probe,[47] and the extent of reduction is maximized at ∼400 °C.[47,65,69−72] Therefore, after *in vacuo* degas at 350 °C prior to water adsorption calorimetry, a large fraction of Cu^{2+} was autoreduced to Cu^{+}. In other words, the near-zero coverage hydration is likely to take place at these under-coordinated Cu^{+} sites with lower *Z*/*r* compared with that of Cu^{2+}. In sum, integrating the TG-DSC-MS and *in situ* DRIFTS data, we confirm the evolution from hydrated and hydroxylated cupric ions to dehydrated cupric ion and copper oxo clusters $[Cu^{2+}{-}O^{2-}{-}Cu^{2+}]^{2+}$, and then to the final decomposition product, cuprous ion species $[Cu^{+}\square Cu^{+}]^{2+}$.

Between 1100 and 800 cm^{-1}, Fe-MOR presents three peaks confirming the presence of confined iron carbonate species (see Figure 5d). Specifically, the peaks at 1024 and 814 cm^{-1} are assigned to the $\nu1$ CO_3^{2-} symmetric stretching[73−77] and $\nu2$ CO_3^{2-} bending modes,[75,77,78] respectively. The peak at 1024 cm^{-1} also suggests that the carbonate is not a free anion, but bound with cations or confined in nanoscale void because the symmetry of free CO_3^{2-} excludes the IR signal at the same wavenumber.[73,74] No shift is observed for these two peaks between 35 and 500 °C. This is in excellent agreement with our TG-DSC-MS data which does not show evidence of carbonate decomposition up to 500 °C. On the other hand, the absorbance at 902 cm^{-1} is assigned to the δ deformation of OH^{-},[78] which red-shifts to lower wavenumbers (874 cm^{-1}) as temperature increases to 200 °C. The intensity of this peak decreases upon further temperature increase up to 500 °C, which reflects dehydration and/or dehydroxylation. The *in situ* DRIFTS results suggest Fe-MOR is the only sample with confined carbonate species, other than the strong coordination affinity iron cation has, probably also due to the more spacious void space of Fe-MOR framework. It has been reported that thermal decomposition of several transition metal hydroxycarbonates also takes place in the temperature range of 500−600 °C.[73,79,80]

Coupling the TG-DSC-MS and *in situ* DRIFTS results shown in Figures 4 and 5, we surmise that the thermal treatment of Cu-MOR under inert gas flow leads to the following stepwise reactions:

(1) *Dehydration* of $[Cu^{2+}OH^{-}]^{+}$ and hydrated Cu^{2+} forming $[Cu^{2+}{-}O^{2-}{-}Cu^{2+}]^{2+}$ clusters and Cu^{2+}, respectively.

$$2[Cu^{2+}OH^{-}]^{+} \rightarrow [Cu^{2+}{-}O^{2-}{-}Cu^{2+}]^{2+} + H_2O \quad \text{(below 200 °C)}$$

$$[Cu^{2+}{\cdot}nH_2O]^{2+} \rightarrow Cu^{2+} + nH_2O \quad \text{(below 200 °C)}$$

(2) *Decomposition* of copper oxo cluster species, according to a recent study by Sushkevich et al.[47] primarily $[Cu^{2+}{-}O^{2-}{-}Cu^{2+}]^{2+}$, leading to liberation of molecular oxygen and formation of $[Cu^{+}\square Cu^{+}]^{2+}$.

https://dx.doi.org/10.1021/acs.jpclett.0c01331
J. Phys. Chem. Lett. 2020, 11, 4774−4784

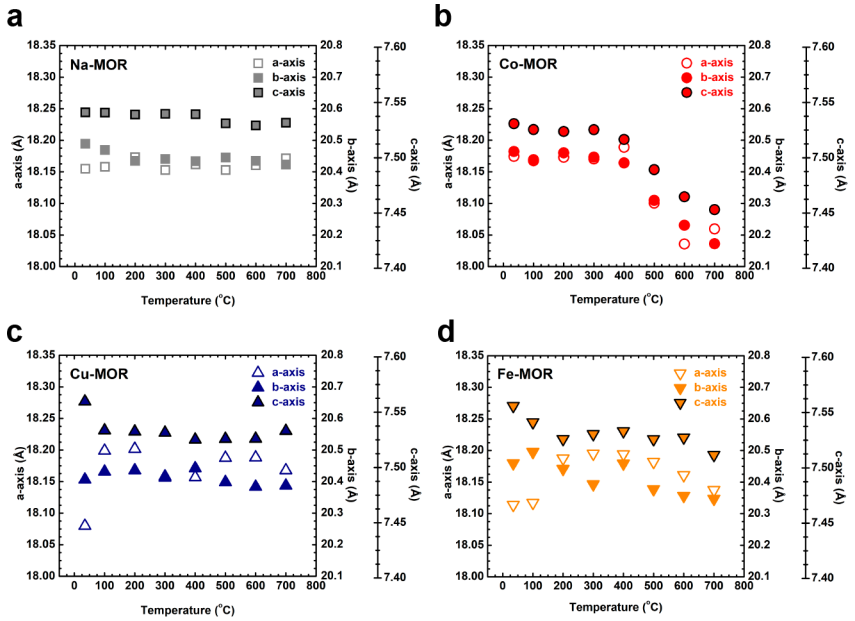

Figure 7. Evolution of lattice parameters for all M-MOR samples as a function of temperature from 35 to 700 °C under helium flow (50 mL/min): (a) Na-MOR, (b) Co-MOR, (c) Cu-MOR, and (d) Fe-MOR.

$$[Cu^{2+}{-}O^{2-}{-}Cu^{2+}]^{2+} \rightarrow \frac{1}{2}O_2 + [Cu^{+}\square Cu^{+}]^{2+} \quad (\sim 915\,^{\circ}C)$$

The presence of copper oxo species is evidenced by the exothermic DSC peak at ∼915 °C and evolution of O_2 gas detected by MS (∼0.2 wt %, see Figure 2e). In addition, we performed TG-DSC-MS thermal analysis on the Cu-MOR sample after water adsorption calorimetry (see Figure S5). The nearly identical TG-DSC-MS profiles highlight the high thermal and hydrothermal stability of copper oxo clusters confined within the MOR framework. Such well-reproduced data strongly support the conclusions by Sushkevich et al. that, energetically, water plays a critical role in regenerating the catalytic sites in Cu-MOR by oxidation of $[Cu^{+}\square Cu^{+}]^{2+}$ to $[Cu^{2+}{-}O^{2-}{-}Cu^{2+}]^{2+}$. To the first-order approximation, the calorimetrically measured $\Delta h_{ads\text{-}zero}$ value (−133.1 ± 6.0 kJ/mol water) of $[Cu^{+}\square Cu^{+}]^{2+}$ hydration within Cu-MOR is consistent with the hydration energetics calculated from their density functional theory (DFT).[47] Moreover, we further demonstrate that the $[Cu^{2+}{-}O^{2-}{-}Cu^{2+}]^{2+}$ site is thermally and hydrothermally stable even under the low oxygen fugacity (anaerobic) MTM reaction conditions.[47]

Unlike Cu-MOR, the MTM (aerobic) catalytic sites in Fe-MOR are zeolitic α-oxygen, which is denoted as $[Fe^{3+}{-}O^{-}]_{\alpha}$.[81,82] These sites are so active that they enable oxidation of methane at room temperature using molecular oxygen; meanwhile, because of such high activity, they also suffer from multiple side reactions and adsorption of impurities. For instance, during the transfer and storage of Fe-exchanged zeolites under ambient conditions, water and CO_2 are easily adsorbed with formation of complex iron species as seen here. There are multiple roles of water, most of which are detrimental to MTM reactions by modification of surface compositions[83−85] and configurations,[86] alteration of reaction pathways, and increase in activation barriers.[83] For example, Panov et al. reported that water can easily convert $[Fe^{3+}{-}O^{-}]_{\alpha}$ to the much less active $[Fe^{3+}{-}OH^{-}]_{\alpha}$.[84] Interestingly, it is also reported that the activation barrier for MTM increases from 28.4 to 54.8 kJ/mol at water vapor pressure as low as 1−100 ppb.[83] By integrating TG-DSC-MS and *in situ* DRIFTS analyses, we confirm the existence of iron carbonate species within Fe-MOR, which are thermally stable up to ∼500 °C. Thus, although the hydration of Fe^{3+} is expected to be energetically favorable and exothermic, this is not seen here by *in situ* adsorption calorimetry probably because of the existence of these multiple stable subnano, confined iron cluster species with significantly reduced *Z/r*, including iron carbonate species that are stable up to ∼500 °C. Therefore, activation of Fe-MOR prior to MTM would be tricky because of the compositional complexity of guest species. We propose a pretreatment temperature greater than 500 °C to completely decompose iron carbonate species for better catalyst performance.

The structural evolutions of all M-MOR samples during thermal treatment from 35 to 700 °C were monitored by *in situ* XRD (see Figure 6). As temperature increases, all samples retain their long-range order up to 700 °C (see Figure S6). The diffraction peaks of each sample right-shift as temperature increases. The *in situ* XRD results reveal systematically evolving lattice parameters and unit cell volume as a function of temperature for each M-MOR (see Figures 7 and 8). In general, the lattice parameters and unit cell volumes both decrease as temperature increases. This is in good agreement with previous reports on other ion-exchanged zeolites, in which thermal treatment between 600 and 850 °C leads to significantly increased cation−framework interactions, accompanied by decreased bond length, modified angles between adjacent tetrahedra, and framework contraction.[61] Strong cluster−framework guest−host interactions are expected for both Cu- and Fe-MOR, mirrored by their expanded frameworks after ion exchange of Na-MOR (see Figure 8). As soon as the iron carbonate species decompose, the unit cell volume of Fe-MOR significantly decreases; however, such a phenomenon is not seen for Cu-MOR which closely hosts copper oxo clusters with high thermal and hydrothermal stability up to at least 900 °C. Further, at 1000 °C *ex situ* XRD patterns in Figure S2 suggest that other than Na-MOR, all three samples

https://dx.doi.org/10.1021/acs.jpclett.0c01331
J. Phys. Chem. Lett. 2020, 11, 4774−4784

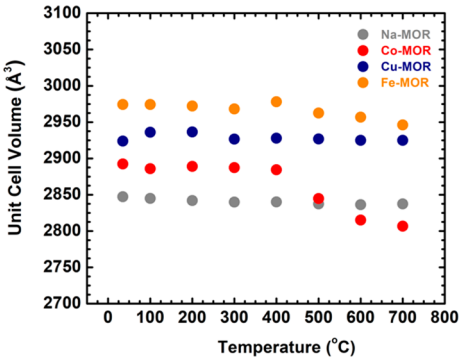

Figure 8. Unit cell volume changes for all M-MOR samples as a function of temperature from 35 to 700 °C under helium flow (50 mL/min).

are amorphized. This highlights the higher thermal stability of MOR with filled or partially filled void space. Although complex DSC peaks were observed between 700 and 800 °C (see Figure 2c), we expect that the amorphous or glassy phase is energetically more stable than the corresponding anhydrous framework structure with the same composition as observed in our earlier study on the energetics and structural evolution of Na−Ca exchanged zeolite A during heating.[87] Our studies focusing on the formation enthalpies of these M-MOR samples, the corresponding amorphous and/or glassy phases, and low-temperature heat capacity are being performed to reveal their energetic stability and intricate cation−framework interactions quantitatively. We will report these results separately in subsequent publications.

In summary, this study leads to the following conclusions closely relevant to selective anaerobic oxidation of methane to methanol using transition metal ion-exchanged mordenites as the catalysts. Most importantly, the near-zero coverage enthalpy of water adsorption reflecting the strongest hydration is more exothermic following the sequence of Fe-, Na-, Cu-, and Co-MOR, which is governed by the type and valency of cationic guest species that determine the average ionic potential (Z/r) of the initial binding sites. We propose that such a site is $[Cu^{+}\square Cu^{+}]^{2+}$ for Cu-MOR, and we speculate for Fe-MOR the binding would be at sites with Fe^{3+} nearly completely coordinated, as indicated by the much less exothermic $\Delta h_{ads\text{-}zero}$. The existence of micropore-confined copper oxo clusters $[Cu^{2+}-O^{2-}-Cu^{2+}]^{2+}$ in Cu-MOR and iron carbonate species in Fe-MOR with high thermal and hydrothermal stability under low oxygen fugacity is determined from integrated TG-DSC-MS and *in situ* DRIFTS analyses, with thermal stability up to ∼915 °C for copper oxo clusters in Cu-MOR and ∼500 °C for iron carbonate species in Fe-MOR. The integral enthalpies of hydration from water adsorption calorimetry are in excellent agreement with the average dehydration enthalpies from thermal analysis. Fe-MOR presents the highest degree of hydration, while Na-MOR has the least. Three stages of thermal evolution (dehydration, guest species decomposition, and framework phase transition) were identified for all samples from room temperature to 1000 °C in an inert atmosphere. The understanding enabled by this study may help us to improve the design of anerobic oxidative MTM reaction processes, from catalyst activation to intermediate stabilization to catalytic site regeneration, by manipulating the oxidation state and coordination chemistry of catalytic centers confined in zeolites with water partial pressure.

EXPERIMENTAL METHODS

Na-MOR was synthesized for further ion-exchange to prepare Co-, Cu-, and Fe-MOR samples. All samples were characterized using inductively coupled plasma-mass spectrometry (ICP-MS) to determine their compositions, *ex situ* powder X-ray diffraction (XRD) for phase identification, and scanning electron microscopy (SEM) for morphology assessment prior to thermal analysis using thermogravimetric analysis−differential scanning calorimetry−mass spectrometry analyses (TG-DSC-MS), water adsorption calorimetry using coupled microcalorimeter and gas adsorption analyzer,[88] *in situ* diffuse reflectance infrared Fourier transform spectroscopy (*in situ* DRIFTS),[89] and *in situ* X-ray diffraction (*in situ* XRD)[89,90] under helium flow at 50 mL/min. Please check the Supporting Information for the details of all experiments performed.

ASSOCIATED CONTENT

Supporting Information

The Supporting Information is available free of charge at https://pubs.acs.org/doi/10.1021/acs.jpclett.0c01331.

Experimental Methods; Results; and additional compositional, spectroscopic, and structural information (PDF)

AUTHOR INFORMATION

Corresponding Authors

Hui Sun − *Petroleum Processing Research Center and International Joint Research Center of Green Energy Chemical Engineering, East China University of Science and Technology, Shanghai 200237, China;* orcid.org/0000-0002-8544-756X; Email: sunhui@ecust.edu.cn

Di Wu − *Alexandra Navrotsky Institute for Experimental Thermodynamics, The Gene and Linda Voiland School of Chemical Engineering and Bioengineering, Department of Chemistry, and Materials Science and Engineering, Washington State University, Pullman, Washington 99163, United States;* orcid.org/0000-0001-6879-321X; Email: d.wu@wsu.edu

Authors

Xianghui Zhang − *Alexandra Navrotsky Institute for Experimental Thermodynamics and The Gene and Linda Voiland School of Chemical Engineering and Bioengineering, Washington State University, Pullman, Washington 99163, United States*

Cody B. Cockreham − *Alexandra Navrotsky Institute for Experimental Thermodynamics and The Gene and Linda Voiland School of Chemical Engineering and Bioengineering, Washington State University, Pullman, Washington 99163, United States; Earth and Environmental Sciences Division, Los Alamos National Laboratory, Los Alamos, New Mexico 87545, United States*

Zhiyang Huang − *Alexandra Navrotsky Institute for Experimental Thermodynamics and The Gene and Linda Voiland School of Chemical Engineering and Bioengineering, Washington State University, Pullman, Washington 99163, United States*

Chen Yang − *Alexandra Navrotsky Institute for Experimental Thermodynamics and The Gene and Linda Voiland School of Chemical Engineering and Bioengineering, Washington State University, Pullman, Washington 99163, United States*

Oscar G. Marin-Flores − *The Gene and Linda Voiland School of Chemical Engineering and Bioengineering, Washington State University, Pullman, Washington 99163, United States*

https://dx.doi.org/10.1021/acs.jpclett.0c01331
J. Phys. Chem. Lett. 2020, 11, 4774−4784

Baodong Wang − *National Institute of Clean-and-Low-Carbon Energy, Beijing 102211, China*

Xiaofeng Guo − *Alexandra Navrotsky Institute for Experimental Thermodynamics, Department of Chemistry, and Materials Science and Engineering, Washington State University, Pullman, Washington 99163, United States;* orcid.org/0000-0003-3129-493X

Su Ha − *The Gene and Linda Voiland School of Chemical Engineering and Bioengineering, Washington State University, Pullman, Washington 99163, United States;* orcid.org/0000-0003-2175-7347

Hongwu Xu − *Earth and Environmental Sciences Division, Los Alamos National Laboratory, Los Alamos, New Mexico 87545, United States*

Complete contact information is available at: https://pubs.acs.org/10.1021/acs.jpclett.0c01331

Notes

The authors declare no competing financial interest.

■ ACKNOWLEDGMENTS

This work was supported by institutional funds from the Gene and Linda Voiland School of Chemical Engineering and Bioengineering and Alexandra Navrotsky Institute for Experimental Thermodynamics at Washington State University. X.Z. was supported by Chambroad Distinguished Scholarship. C.B.C. received support from the Achievement Rewards for College Scientists (ARCS) Fellowship from the ARCS Seattle Chapter. H.S. acknowledges funds from the National Natural Science Foundation of China (Grants 91634112 and 21878097) and the Natural Science Foundation of Shanghai (Grant 16ZR1408100). We thank Hao Jiang for graphing the illustrated zeolite structures.

■ REFERENCES

(1) Schwach, P.; Pan, X.; Bao, X. Direct Conversion of Methane to Value-Added Chemicals over Heterogeneous Catalysts: Challenges and Prospects. *Chem. Rev.* **2017**, *117*, 8497−8520.

(2) Tang, P.; Zhu, Q.; Wu, Z.; Ma, D. Methane Activation: The Past and Future. *Energy Environ. Sci.* **2014**, *7*, 2580−2591.

(3) Olivos-Suarez, A. I.; Szécsényi, À.; Hensen, E. J. M.; Ruiz-Martinez, J.; Pidko, E. A.; Gascon, J. Strategies for the Direct Catalytic Valorization of Methane Using Heterogeneous Catalysis: Challenges and Opportunities. *ACS Catal.* **2016**, *6*, 2965−2981.

(4) Tomkins, P.; Ranocchiari, M.; Van Bokhoven, J. A. Direct Conversion of Methane to Methanol under Mild Conditions over Cu-Zeolites and Beyond. *Acc. Chem. Res.* **2017**, *50*, 418−425.

(5) Taifan, W.; Baltrusaitis, J. CH4 Conversion to Value Added Products: Potential, Limitations and Extensions of a Single Step Heterogeneous Catalysis. *Appl. Catal., B* **2016**, *198*, 525−547.

(6) Reddy, P. V. L.; Kim, K. H.; Song, H. Emerging Green Chemical Technologies for the Conversion of CH4 to Value Added Products. *Renewable Sustainable Energy Rev.* **2013**, *24*, 578−585.

(7) Xie, S.; Lin, S.; Zhang, Q.; Tian, Z.; Wang, Y. Selective Electrocatalytic Conversion of Methane to Fuels and Chemicals. *J. Energy Chem.* **2018**, *27*, 1629−1636.

(8) Banerjee, R.; Proshlyakov, Y.; Lipscomb, J. D.; Proshlyakov, D. A. Structure of the Key Species in the Enzymatic Oxidation of Methane to Methanol. *Nature* **2015**, *518*, 431−434.

(9) Rosenzweig, A. C.; Frederick, C. A.; Lippard, S. J.; Nordlund, P. Crystal Structure of a Bacterial Non-Haem Iron Hydroxylase That Catalyses the Biological Oxidation of Methane. *Nature* **1993**, *366*, 537−543.

(10) Sirajuddin, S.; Rosenzweig, A. C. Enzymatic Oxidation of Methane. *Biochemistry* **2015**, *54*, 2283−2294.

(11) Bordeaux, M.; Galarneau, A.; Drone, J. Catalytic, Mild, and Selective Oxyfunctionalization of Linear Alkanes: Current Challenges. *Angew. Chem., Int. Ed.* **2012**, *51*, 10712−10723.

(12) Ro, S. Y.; Schachner, L. F.; Koo, C. W.; Purohist, R.; Remis, J. P.; Kenney, G. E.; Liauw, B. W.; Thomas, P. M.; Patrie, S. M.; Kelleher, N. L. Native Top-down Mass Spectrometry Provides Insights into the Copper Centers of Membrane-Bound Methane Monooxygenase. *Nat. Commun.* **2019**, *10*, 1−12.

(13) Park, M. B.; Park, E. D.; Ahn, W.-S. Recent Progress in Direct Conversion of Methane to Methanol Over Copper-Exchanged Zeolites. *Front. Chem.* **2019**, *7*, 1−7.

(14) Göltl, F.; Michel, C.; Andrikopoulos, P. C.; Love, A. M.; Hafner, J.; Hermans, I.; Sautet, P. Computationally Exploring Confinement Effects in the Methane-to-Methanol Conversion over Iron-Oxo Centers in Zeolites. *ACS Catal.* **2016**, *6*, 8404−8409.

(15) Dinh, K. T.; Sullivan, M. M.; Serna, P.; Meyer, R. J.; Dincă, M.; Román-Leshkov, Y. Viewpoint on the Partial Oxidation of Methane to Methanol Using Cu- and Fe-Exchanged Zeolites. *ACS Catal.* **2018**, *8*, 8306−8313.

(16) Park, M. B.; Ahn, S. H.; Mansouri, A.; Ranocchiari, M.; van Bokhoven, J. A. Comparative Study of Diverse Copper Zeolites for the Conversion of Methane into Methanol. *ChemCatChem* **2017**, *9*, 3705−3713.

(17) Mahyuddin, M. H.; Staykov, A.; Shiota, Y.; Miyanishi, M.; Yoshizawa, K. Roles of Zeolite Confinement and Cu-O-Cu Angle on the Direct Conversion of Methane to Methanol by [Cu2(μ-O)]2+-Exchanged AEI, CHA, AFX, and MFI Zeolites. *ACS Catal.* **2017**, *7*, 3741−3751.

(18) Narsimhan, K.; Iyoki, K.; Dinh, K.; Román-Leshkov, Y. Catalytic Oxidation of Methane into Methanol over Copper-Exchanged Zeolites with Oxygen at Low Temperature. *ACS Cent. Sci.* **2016**, *2*, 424−429.

(19) Snyder, B. E. R.; Vanelderen, P.; Bols, M. L.; Hallaert, S. D.; Böttger, L. H.; Ungur, L.; Pierloot, K.; Schoonheydt, R. A.; Sels, B. F.; Solomon, E. I. The Active Site of Low-Temperature Methane Hydroxylation in Iron-Containing Zeolites. *Nature* **2016**, *536*, 317−321.

(20) Li, G.; Sun, H.; Xu, H.; Guo, X.; Wu, D. Probing the Energetics of Molecule-Material Interactions at Interfaces and in Nanopores. *J. Phys. Chem. C* **2017**, *121* (39), 26141.

(21) Shi, Y.; Liu, S.; Liu, Y.; Huang, W.; Guan, G.; Zuo, Z. Quasicatalytic and Catalytic Selective Oxidation of Methane to Methanol over Solid Materials: A Review on the Roles of Water. *Catal. Rev.: Sci. Eng.* **2019**, *00*, 1−33.

(22) Ravi, M.; Ranocchiari, M.; van Bokhoven, J. A. The Direct Catalytic Oxidation of Methane to Methanol—A Critical Assessment. *Angew. Chem., Int. Ed.* **2017**, *56*, 16464−16483.

(23) Kulkarni, A. R.; Zhao, Z. J.; Siahrostami, S.; Nørskov, J. K.; Studt, F. Cation-Exchanged Zeolites for the Selective Oxidation of Methane to Methanol. *Catal. Sci. Technol.* **2018**, *8*, 114−123.

(24) Ravi, M.; Sushkevich, V. L.; Knorpp, A. J.; Newton, M. A.; Palagin, D.; Pinar, A. B.; Ranocchiari, M.; van Bokhoven, J. A. Misconceptions and Challenges in Methane-to-Methanol over Transition-Metal-Exchanged Zeolites. *Nat. Catal.* **2019**, *2*, 485−494.

(25) Taarning, E.; Osmundsen, C. M.; Yang, X.; Voss, B.; Andersen, S. I.; Christensen, C. H. Zeolite-Catalyzed Biomass Conversion to Fuels and Chemicals. *Energy Environ. Sci.* **2011**, *4*, 793−804.

(26) Li, J. P. H.; Kennedy, E.; Stockenhuber, M. Oxidative Coupling and Hydroxylation of Phenol over Transition Metal and Acidic Zeolites: Insights into Catalyst Function. *Catal. Lett.* **2014**, *144*, 9−15.

(27) Buchireddy, P. R.; Bricka, R. M.; Rodriguez, J.; Holmes, W. Biomass Gasification: Catalytic Removal of Tars over Zeolites and Nickel Supported Zeolites. *Energy Fuels* **2010**, *24*, 2707−2715.

(28) Li, P.; Li, D.; Yang, H.; Wang, X.; Chen, H. Effects of Fe-, Zr-, and Co-Modified Zeolites and Pretreatments on Catalytic Upgrading of Biomass Fast Pyrolysis Vapors. *Energy Fuels* **2016**, *30*, 3004−3013.

(29) Rahman, M. M.; Liu, R.; Cai, J. Catalytic Fast Pyrolysis of Biomass over Zeolites for High Quality Bio-Oil − A Review. *Fuel Process. Technol.* **2018**, *180*, 32−46.

(30) Fedeyko, J. M.; Chen, B.; Chen, H. Y. Mechanistic Study of the Low Temperature Activity of Transition Metal Exchanged Zeolite SCR Catalysts. *Catal. Today* **2010**, *151*, 231−236.
(31) Cant, N. W.; Liu, I. O. Y. Mechanism of the Selective Reduction of Nitrogen Oxides by Hydrocarbons on Zeolite Catalysts. *Catal. Today* **2000**, *63*, 133−146.
(32) Brandenberger, S.; Kröcher, O.; Tissler, A.; Althoff, R. The State of the Art in Selective Catalytic Reduction of NOx by Ammonia Using Metal-Exchanged Zeolite Catalysts. *Catal. Rev.: Sci. Eng.* **2008**, *50*, 492.
(33) Epling, W. S.; Campbell, L. E.; Yezerets, A.; Currier, N. W.; Parks, J. E. Overview of the Fundamental Reactions and Degradation Mechanisms of NOx Storage/Reduction Catalysts. *Catal. Rev.: Sci. Eng.* **2004**, *46*, 163−245.
(34) Sirijaruphan, A.; Horváth, A.; Goodwin, J. G.; Oukaci, R. Cobalt Aluminate Formation in Alumina-Supported Cobalt Catalysts: Effects of Cobalt Reduction State and Water Vapor. *Catal. Lett.* **2003**, *91*, 89−94.
(35) Guillemot, M.; Mijoin, J.; Mignard, S.; Magnoux, P. Adsorption of Tetrachloroethylene on Cationic X and Y Zeolites: Influence of Cation Nature and of Water Vapor. *Ind. Eng. Chem. Res.* **2007**, *46*, 4614−4620.
(36) Chen, K.; Damron, J.; Pearson, C.; Resasco, D.; Zhang, L.; White, J. L. Zeolite Catalysis: Water Can Dramatically Increase or Suppress Alkane C-H Bond Activation. *ACS Catal.* **2014**, *4*, 3039−3044.
(37) Okuhara, T. Water-Tolerant Solid Acid Catalysts. *Chem. Rev.* **2002**, *102*, 3641−3666.
(38) Čapek, L.; Dědeček, J.; Wichterlová, B. Co-Beta Zeolite Highly Active in Propane-SCR-NOx in the Presence of Water Vapor: Effect of Zeolite Preparation and A1 Distribution in the Framework. *J. Catal.* **2004**, *227*, 352−366.
(39) Chen, L.; Si, Z.; Wu, X.; Weng, D.; Wu, Z. Effect of Water Vapor on NH3-NO/NO2 SCR Performance of Fresh and Aged MnOx-NbOx-CeO2 Catalysts. *J. Environ. Sci. (Beijing, China)* **2015**, *31*, 240−247.
(40) Jehng, J. M.; Deo, G.; Weckhuysen, B. M.; Wachs, I. E. Effect of Water Vapor on the Molecular Structures of Supported Vanadium Oxide Catalysts at Elevated Temperatures. *J. Mol. Catal. A: Chem.* **1996**, *110*, 41−54.
(41) Hibbitts, D. D.; Loveless, B. T.; Neurock, M.; Iglesia, E. Mechanistic Role of Water on the Rate and Selectivity of Fischer−Tropsch Synthesis on Ruthenium Catalysts. *Angew. Chem., Int. Ed.* **2013**, *52*, 12273−12278.
(42) Zhao, Z.; Xu, S.; Hu, M. Y.; Bao, X.; Peden, C. H. F.; Hu, J. Investigation of Aluminum Site Changes of Dehydrated Zeolite H-Beta during a Rehydration Process by High-Field Solid-State NMR. *J. Phys. Chem. C* **2015**, *119*, 1410−1417.
(43) De Wispelaere, K.; Hemelsoet, K.; Waroquier, M.; Van Speybroeck, V. Complete Low-Barrier Side-Chain Route for Olefin Formation during Methanol Conversion in H-SAPO-34. *J. Catal.* **2013**, *305*, 76−80.
(44) Chen, K.; Kelsey, J.; White, J. L.; Zhang, L.; Resasco, D. Water Interactions in Zeolite Catalysts and Their Hydrophobically Modified Analogues. *ACS Catal.* **2015**, *5*, 7480−7487.
(45) Wu, X.; Anthony, R. G. Effect of Feed Composition on Methanol Conversion to Light Olefins over SAPO-34. *Appl. Catal., A* **2001**, *218*, 241−250.
(46) van Niekerk, M. J.; Fletcher, J. C.Q.; O'Connor, C. T. Effect of Catalyst Modification on the Conversion of Methanol to Light Olefins over SAPO-34. *Appl. Catal., A* **1996**, *138*, 135−145.
(47) Sushkevich, V. L.; Palagin, D.; Ranocchiari, M.; van Bokhoven, J. A. Selective Anaerobic Oxidation of Methane Enables Direct Synthesis Ofmethanol. *Science (Washington, DC, U. S.)* **2017**, *356* (5), 523−527.
(48) Newton, M. A.; Knorpp, A. J.; Pinar, A. B.; Sushkevich, V. L.; Palagin, D.; Van Bokhoven, J. A. On the Mechanism Underlying the Direct Conversion of Methane to Methanol by Copper Hosted in Zeolites; Braiding Cu K-Edge XANES and Reactivity Studies. *J. Am. Chem. Soc.* **2018**, *140*, 10090.
(49) Sushkevich, V. L.; Palagin, D.; Ranocchiari, M.; Van Bokhoven, J. A. Selective Anaerobic Oxidation of Methane Enables Direct Synthesis of Methanol. *Science (Washington, DC, U. S.)* **2017**, *356*, 523.
(50) Navrotsky, A.; Tian, Z. R. Systematics in the Enthalpies of Formation of Anhydrous Aluminosilicate Zeolites, Glasses, and Dense Phases. *Chem. - Eur. J.* **2001**, *7*, 769−774.
(51) Sun, H.; Wu, D.; Liu, K.; Guo, X.; Navrotsky, A. Energetics of Alkali and Alkaline Earth Ion-Exchanged Zeolite A. *J. Phys. Chem. C* **2016**, *120*, 15251−15256.
(52) Sun, H.; Wu, D.; Guo, X.; Shen, B.; Navrotsky, A. Energetics of Sodium-Calcium Exchanged Zeolite A. *Phys. Chem. Chem. Phys.* **2015**, *17*, 11198.
(53) Sun, P.; Navrotsky, A. Enthalpy of Formation and Dehydration of Alkaline Earth Cation Exchanged Zeolite Beta. *Microporous Mesoporous Mater.* **2008**, *109*, 147−155.
(54) Yang, S.; Navrotsky, A. Energetics of Formation and Hydration of Ion-Exchanged Zeolite Y. *Microporous Mesoporous Mater.* **2000**, *37*, 175−186.
(55) Wu, L.; Navrotsky, A.; Lee, Y.; Lee, Y. Thermodynamic Study of Alkali and Alkaline-Earth Cation-Exchanged Natrolites. *Microporous Mesoporous Mater.* **2013**, *167*, 221−227.
(56) Navrotsky, A.; Trofymluk, O.; Levchenko, A. A. Thermochemistry of Microporous and Mesoporous Materials. *Chem. Rev.* **2009**, *109*, 3885.
(57) Radha, A. V.; Forbes, T. Z.; Killian, C. E.; Gilbert, P. U. P. A.; Navrotsky, A. Transformation and Crystallization Energetics of Synthetic and Biogenic Amorphous Calcium Carbonate. *Proc. Natl. Acad. Sci. U. S. A.* **2010**, *107*, 16438.
(58) Radha, A. V.; Navrotsky, A. Direct Experimental Measurement of Water Interaction Energetics in Amorphous Carbonates MCO3 (M = Ca, Mn, and Mg) and Implications for Carbonate Crystal Growth. *Cryst. Growth Des.* **2015**, *15*, 70.
(59) Sel, O.; Radha, A. V.; Dideriksen, K.; Navrotsky, A. Amorphous Iron (II) Carbonate: Crystallization Energetics and Comparison to Other Carbonate Minerals Related to CO 2 Sequestration. *Geochim. Cosmochim. Acta* **2012**, *87*, 61.
(60) Sun, P.; Deore, S.; Navrotsky, A. Enthalpy of Formation and Dehydration of Lithium and Sodium Zeolite Beta. *Microporous Mesoporous Mater.* **2007**, *98*, 29−40.
(61) Martucci, A.; Sacerdoti, M.; Cruciani, G.; Dalconi, C. In Situ Time Resolved Synchrotron Powder Diffraction Study of Mordenite. *Eur. J. Mineral.* **2003**, *15* (3), 485−493.
(62) Zecchina, A.; Bordiga, S.; Lamberti, C.; Ricchiardi, G.; Lamberti, C.; Ricchiardi, G.; Scarano, D.; Petrini, G.; Leofanti, G.; Mantegazza, M. Structural Characterization of Ti Centres in Ti-Silicalite and Reaction Mechanisms in Cyclohexanone Ammoximation. *Catal. Today* **1996**, *32*, 97−106.
(63) Sobalík, Z.; Tvarůžková, Z.; Wichterlová, B. Skeletal T-O-T Vibrations as a Tool for Characterization of Divalent Cation Complexation in Ferrierite. *J. Phys. Chem. B* **1998**, *102*, 1077−1085.
(64) Sárkány, J.; Sachtler, W. M. H. Redox Chemistry of Cu NaZSM-5: Detection of Cuprous Ions by FTi.R. *Zeolites* **1994**, *14*, 7−11.
(65) Turnes Palomino, G.; Fisicaro, P.; Bordiga, S.; Zecchina, A.; Giamello, E.; Lamberti, C. Oxidation States of Copper Ions in ZSM-5 Zeolites. A Multitechnique Investigation. *J. Phys. Chem. B* **2000**, *104* (17), 4064−4073.
(66) Scarano, D.; Zecchina, A.; Bordiga, S.; Geobaldo, F.; Spoto, G.; Petrini, G.; Leofanti, G.; Padovan, M.; Tozzola, G. Fourier-Transform Infrared and Raman Spectra of Pure and Al-, B-, Ti- and Fe-Substituted Silicalites . *J. Chem. Soc., Faraday Trans.* **1993**, *89*, 4123−4130.
(67) Lei, G. D.; Adelman, B. J.; Sárkány, J.; Sachtler, W. M. H. Identification of Copper(II) and Copper(I) and Their Interconversion in Cu/ZSM-5 De-NOx Catalysts. *Appl. Catal., B* **1995**, *5*, 245−256.

https://dx.doi.org/10.1021/acs.jpclett.0c01331
J. Phys. Chem. Lett. 2020, 11, 4774−4784

(68) Sárkány, J. FTIR Study on the Interaction of O2 and CO with Cu+ Ions in Zeolite ZSM-5. Formation and Reactivity of Superoxide. *J. Mol. Struct.* **1997**, *410*−*411*, 95−98.
(69) Jacobs, W. P. J. H.; van Wolput, J. H. M. C.; van Santen, R. A. An in Situ Fourier Transform Infrared Studyof Zeolitic Vibrations: Dehydration, Deammoniation, and Reammoniation of Ion-Exchanged Y Zeolites. *Zeolites* **1993**, *13*, 170−182.
(70) Kuroda, Y.; Yoshikawa, Y.; Konno, S. I.; Hamano, H.; Maeda, H.; Kumashiro, R.; Nagao, M. Specific Feature of Copper Ion-Exchanged Mordenite for Dinitrogen Adsorption at Room Temperature. *J. Phys. Chem.* **1995**, *99* (26), 10621−10628.
(71) Larsen, S. C.; Aylor, A.; Bell, A. T.; Reimer, J. A. Electron Paramagnetic Resonance Studies of Copper Ion-Exchanged ZSM-5. *J. Phys. Chem.* **1994**, *98* (44), 11533−11540.
(72) Llabrés i Xamena, F. X.; Fisicaro, P.; Berlier, G.; Zecchina, A.; Palomino, G. T.; Prestipino, C.; Bordiga, S.; Giamello, E.; Lamberti, C. Thermal Reduction of Cu2+-Mordenite and Re-Oxidation upon Interaction with H2O, O2, and NO. *J. Phys. Chem. B* **2003**, *107*, 7036−7044.
(73) Shtertser, N. V.; Plyasova, L. M.; Dokuchits, E. V.; Minyukova, T. P.; Yurieva, T. M. Thermal Decomposition of Hydroxycarbonate Cu-Fe-Cr Spinel Precursors. *Catal. Sustainable Energy* **2017**, *4*, 67−72.
(74) Amonette, J. E. Identification of Noncrystalline $(Fe,Cr)(OH)_3$ By Infrared Spectroscopy. *Clays Clay Miner.* **1990**, *38*, 129−136.
(75) Pandarinathan, V.; Lepková, K.; van Bronswijk, W. Chukanovite (Fe2(OH)2CO3) Identified as a Corrosion Product at Sand-Deposited Carbon Steel in CO2-Saturated Brine. *Corros. Sci.* **2014**, *85*, 26−32.
(76) Winkel, K.; Hage, W.; Loerting, T.; Price, S. L.; Mayer, E. Carbonic Acid: From Polyamorphism to Polymorphism. *J. Am. Chem. Soc.* **2007**, *129* (45), 13863−13871.
(77) Kohl, I.; Winkel, K.; Bauer, M.; Liedl, K. R.; Loerting, T.; Mayer, E. Raman Spectroscopic Study of the Phase Transition of Amorphous to Crystalline β-Carbonic Acid. *Angew. Chem., Int. Ed.* **2009**, *48* (15), 2690−2694.
(78) Rémazeilles, C.; Refait, P. Fe(II) Hydroxycarbonate Fe2(OH)-2CO3 (Chukanovite) as Iron Corrosion Product: Synthesis and Study by Fourier Transform Infrared Spectroscopy. *Polyhedron* **2009**, *28*, 749−756.
(79) Ginés, M. J. L.; Apesteguía, C. R. Thermal Decomposition of Cu-Based Hydroxycarbonate Catalytic Precursors for the Low-Temperature CO-Shift Reaction. *J. Therm. Anal.* **1997**, *50*, 745−756.
(80) Kowalik, P.; Konkol, M.; Kondracka, M.; Próchniak, W.; Bicki, R.; Wiercioch, P. The CuZnZrAl Hydroxycarbonates as Copper Catalyst Precursors - Structure, Thermal Decomposition and Reduction Studies. *Appl. Catal., A* **2013**, *452*, 139−146.
(81) Knops-Gerrits, P. P.; Goddard, W. A. Methane Partial Oxidation in Iron Zeolites: Theory versus Experiment. *J. Mol. Catal. A: Chem.* **2001**, *166* (1), 135−145.
(82) Knops-Gerrits, P. P.; Smith, W. J. Methane Partial Oxidation in New Iron Zeolite Topologies. *Stud. Surf. Sci. Catal.* **2000**, *130*, 3531−3536.
(83) Heyden, A.; Peters, B.; Bell, A. T.; Keil, F. J. Comprehensive DFT Study of Nitrous Oxide Decomposition over Fe-ZSM-5. *J. Phys. Chem. B* **2005**, *109* (5), 1857−1873.
(84) Panov, G. I.; Starokon, E. V.; Pirutko, L. V.; Paukshtis, E. A.; Parmon, V. N. New Reaction of Anion Radicals O- with Water on the Surface of FeZSM-5. *J. Catal.* **2008**, *254* (1), 110−120.
(85) Bulushev, D. A.; Prechtl, P. M.; Renken, A.; Kiwi-Minsker, L. Water Vapor Effects in N2O Decomposition over Fe-ZSM-5 Catalysts with Low Iron Content. *Ind. Eng. Chem. Res.* **2007**, *46* (12), 4178−4185.
(86) Zhu, Q.; Hensen, E. J. M.; Mojet, B. L.; van Wolput, J. H. M. C.; van Santen, R. A. N2O Decomposition over Fe/ZSM-5: Reversible Generation of Highly Active Cationic Fe Species. *Chem. Commun.* **2002**, *2* (11), 1232−1233.
(87) Sun, H.; Wu, D.; Guo, X.; Navrotsky, A. Energetics and Structural Evolution of Na-Ca Exchanged Zeolite A during Heating. *Phys. Chem. Chem. Phys.* **2015**, *17*, 9241.
(88) Wang, J.; Yilmaz, E.; Zhang, X.; Li, H.; Zhang, R.; Guo, X.; Sun, H.; Wang, B.; Wu, D. Hydration Energetics of a Diamine-Appended Metal-Organic Framework Carbon Capture Sorbent. *J. Phys. Chem. C* **2020**, *124*, 398.
(89) Zhang, X.; Cockreham, C. B.; Yilmaz, E.; Li, G.; Li, N.; Ha, S.; Fu, L.; Qi, J.; Xu, H.; Wu, D. Energetic Cost for Being "Redox-Site-Rich" in Pseudocapacitive Energy Storage with Nickel − Aluminum Layered Double Hydroxide Materials. *J. Phys. Chem. Lett.* **2020**, *11*, 3745.
(90) Cockreham, C.; Zhang, X.; Li, H.; Hammond-Pereira, E.; Sun, J.; Saunders, S. R.; Wang, Y.; Xu, H.; Wu, D. Inhibition of AlF3·3H2O Impurity Formation in Ti3C2Tx MXene Synthesis under a Unique CoFx/HCl Etching Environment. *ACS Appl. Energy Mater.* **2019**, *2*, 8145.

https://dx.doi.org/10.1021/acs.jpclett.0c01331
J. Phys. Chem. Lett. 2020, 11, 4774−4784